

Biomechanical Effects of Scaphotrapeziotrapezoid (STT) Arthrodesis: A Finite Element Analysis Study

Andres Mena¹[0000-0002-1125-8184], Ronit Wollstein²[0000-0001-9092-3930]

and James Yang¹[0000-0003-0842-7933]

¹ Texas Tech University, Lubbock TX 79409, USA

² University of Alabama at Birmingham, Birmingham AL 35294, USA
james.yang@ttu.edu

Abstract. Scaphotrapeziotrapezoid (STT) arthrodesis is a surgical procedure used to treat various wrist pathologies, yet its biomechanical implications remain incompletely understood. This study investigates the effects of STT fusion on wrist biomechanics using a validated finite element model. Building upon a previously validated whole-wrist finite element model developed from CT scans of a 68-year-old male type I wrist, we simulated STT arthrodesis by creating a unified bone complex comprising the scaphoid, trapezium, and trapezoid, including filled articular spaces. The model was analyzed under physiological grasping loads, examining both radial and ulnar axial load distributions and articular contact pressures at the radioscaphoid and radiolunate interfaces. The fused STT complex becomes a major load-bearing structure, while radiocarpal contact pressures at both the radioscaphoid and radiolunate interfaces show reductions compared to the healthy model. This altered load distribution pattern suggests significant biomechanical adaptations following the procedure. The comparative analyses between healthy and fused models provide valuable insights into post-surgical wrist mechanics, potentially aiding surgical planning. Our findings contribute to the understanding of post-arthrodesis carpal load transfer mechanisms and their clinical implications.

Keywords: Wrist Biomechanics, STT arthrodesis, Finite Element Analysis, Joint Fusion.

1 Introduction

Fusion or arthrodesis of the scaphotrapeziotrapezoid (STT) joint was described by Watson et al. in 1980 [1]. This procedure has been used for the treatment of scapholunate instability, Kienbock's disease (along with lunate implants) and most reliably for STT joint osteoarthritis [2], [3], [4]. The results have been mixed with unclear outcomes and a high nonunion rate; therefore, this has remained a controversial procedure [5], [6], [7], [8], [9], [10]. The techniques for obtaining fusion have evolved and include arthroscopic techniques as well as the use of different types of fixation devices [3], [4]. It is possible that these can lower the incidence of nonunion, but studies are still limited.

Alternative treatments for STT arthritis have been proposed but each has its limitations. Excision of the distal pole of the scaphoid can produce midcarpal instability, while implant arthroplasties can dislocate and their long-term results are still unknown [11], [12].

The biomechanical effect of this limited arthrodesis remains unclear. Short et al. using a cadaver model demonstrated that an STT joint fusion with the scaphoid in a neutral or extended position unloads the lunate fossa and shifts the load to the radioscaphoid joint [13]. Understanding the transfer of forces through the wrist in the presence of an STT joint arthrodesis can allow us to predict the surgical outcome, and better tailor a procedure to a specific wrist/patient. The purpose of this study was to use a previously established finite element (FE) model of the wrist to study the mechanical effect of STT joint fusion, specifically comparing the transfer of forces through the midcarpal joint before and after arthrodesis for a type I lunate wrist.

We hypothesize that STT joint arthrodesis will affect transfer of forces through the radiocarpal joint, and that the transfer of forces will behave differently depending on midcarpal joint structure.

2 Material and Methods

2.1 Base Finite Element Model

This study builds upon a previously validated finite element model of the human wrist [14]. Briefly, the base model was constructed from CT scans (0.6-mm slices) of a 68-year-old male with a type I lunate wrist [15], [16]. The model incorporated all relevant wrist structures including the distal ends of the radius and ulna, eight carpal bones, and the proximal portions of five metacarpals. The base model represented bone tissue using a combination of hexahedral elements for trabecular bone (linear stress-constant solid elements) and quadrilateral shell elements (Tsay-Belytschko formulation) for cortical bone, with thicknesses of 1 mm for carpal bones and 2 mm for long bones. Cartilage was modeled using thick shell elements at articulating surfaces, and a total of 62 ligaments were originally implemented using multiple linear springs. All tissues were modeled using linear elastic material properties, with values of 17,500 MPa (Young's modulus) and 0.3 (Poisson's ratio) for cortical bone, 600 MPa and 0.12 for trabecular bone, and 6 MPa and 0.49 for cartilage. Contact between structures was defined using a penalty-based surface-to-surface algorithm. Further details regarding the base model development and validation are available in Mena et al. [14].

2.2 STT Arthrodesis Model Development

To simulate the scaphotrapeziotrapezoid (STT) arthrodesis, significant modifications were made to the base model. The scaphoid, trapezium, and trapezoid were removed from the original model, along with their associated articular cartilage surfaces. A new bone complex representing the fused STT joint was created in 3D Slicer [17], [18] using the original patient's CT scan. This STT bone complex was formed by merging the

volumes of the scaphoid, trapezium, and trapezoid (original combined volume: 9086.61 mm³) and filling the articular spaces between them, resulting in a final volume of 9938.42 mm³ – a 9.37% increase from the original bones' volume.

The material properties assigned to the fused STT complex remained consistent with the other carpal bones, maintaining the same cortical and trabecular bone properties. The solid-shell element architecture was preserved to ensure consistent mechanical behavior across the modified model.

The fusion model also required modifications to the ligaments. Four ligaments connecting the now-fused bones were removed completely: scaphoid-trapezium (dorsal and palmar) and trapezoid-trapezium (dorsal and palmar). Additionally, 13 ligaments that were originally connected to one of the STT bones were reattached to appropriate locations on the new fused complex, maintaining their original second connection. These included: scapholunate, radioscaphoid, scaphoid-triquetrum, and multiple ligaments connecting the trapezium and trapezoid to the metacarpals and the capitate. The stiffness properties of these reattached ligaments remained unchanged from the base model.

2.3 Loading and Boundary Conditions

The boundary conditions and loading scenarios remained identical to those used for validating the base model's grasping simulation. Forces were applied to the distal surfaces of the metacarpals using the complete force components (Fx, Fy, Fz) as specified in the original model validation [14]. The proximal ends of the radius and ulna were fully constrained, while the metacarpal surfaces were constrained in the x and y directions, allowing movement only along the proximal-distal (z) axis.

2.4 Validation and Verification

The model was analyzed using LS-DYNA explicit solver R14.0 with double precision. Quasi-static conditions were maintained throughout the simulation, with kinetic energy remaining below 5% of the internal energy. The primary metrics evaluated to assess the biomechanical effects of STT arthrodesis included: (i) radial and ulnar axial force distribution, (ii) peak radiocarpal contact pressures at the radioscaphoid and radiolunate interfaces. Additionally, stress and nodal displacement contours were analyzed to identify force transfer patterns throughout the carpal complex. These metrics allowed for direct comparison between the healthy wrist model and the STT arthrodesis model, providing insights into the biomechanical changes introduced by the fusion procedure.

3 Results

3.1 Radial and Ulnar Axial Force Distribution

Following STT arthrodesis, the radial axial force distribution during metacarpal-driven grasping showed a slight increase from 86.05% in the healthy model to 87.98% in the

STT fusion model (**Fig. 1**). This suggests that despite the significant structural modification of the STT complex, the overall distribution of axial forces through the radius and ulna remains relatively consistent. This finding also aligns with previous computational and cadaveric studies that consistently demonstrate predominant radial force transmission during grasping activities [19], [20], [21], [22].

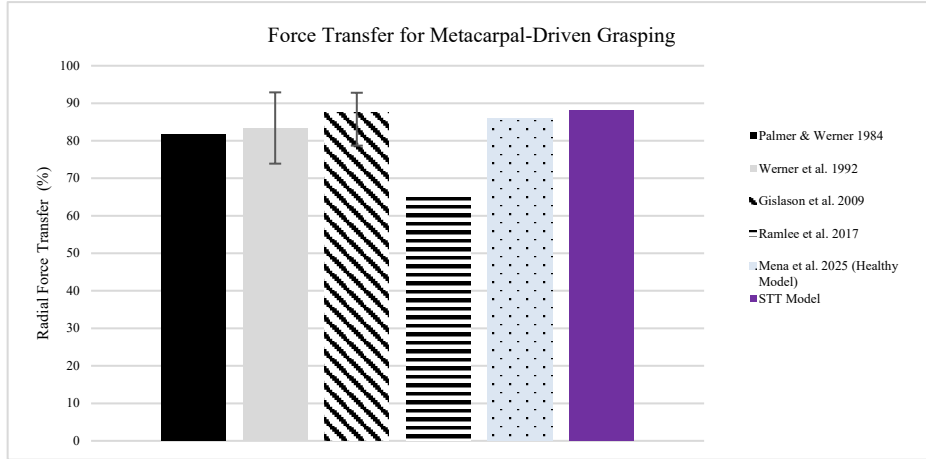


Fig. 1. Comparison of radial axial force transfer of STT model with the literature

3.2 Radiocarpal Contact Mechanics

Peak articular contact pressures at the radiocarpal interface showed notable changes following STT arthrodesis **Fig. 2**. For clarity, in the STT fusion model, the term "radioscaphoid articulation" refers to the contact interface between the radius and the scaphoid portion of the fused STT complex, while "radiolunate articulation" maintains its conventional definition.

At the radioscaphoid articulation, peak contact pressure decreased from 7.5 MPa in the healthy model to 3.8 MPa in the STT fusion model, representing a 49.3% reduction. Similarly, radiolunate peak pressure decreased from 5.0 MPa to 4.4 MPa, a 12.0% reduction. These findings indicate a significant redistribution of contact forces at the radiocarpal interface following STT fusion.

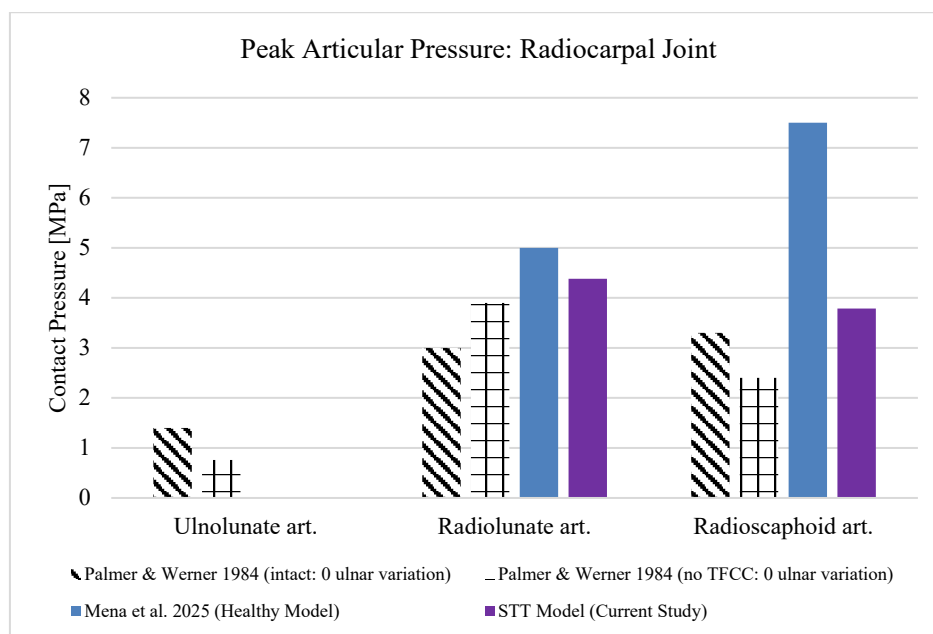
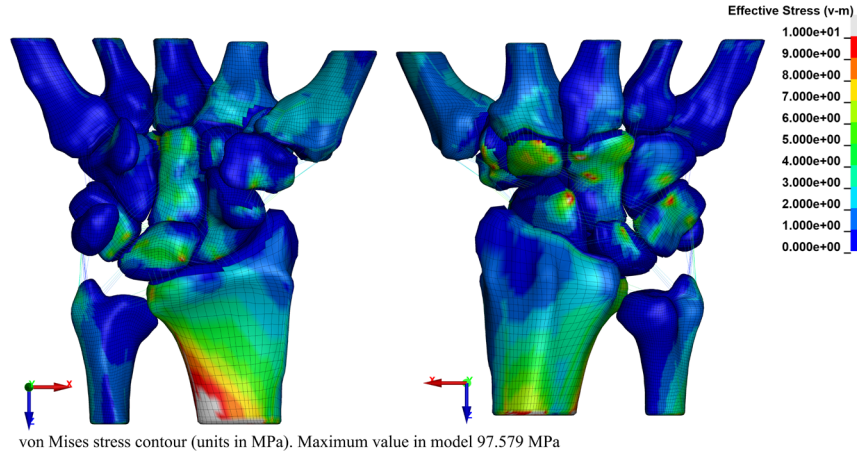


Fig. 2. Comparison of peak articular pressure for the radiocarpal articulations

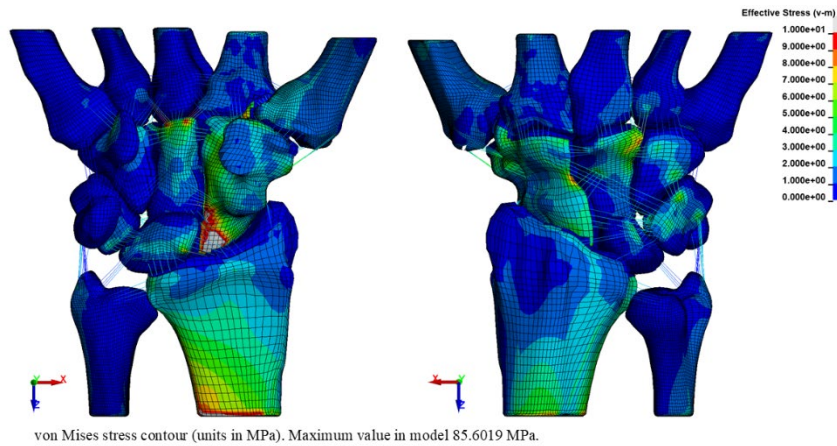
3.3 Stress Distribution and Displacement Patterns

Von Mises stress contours reveal interesting changes in force transmission pathways following STT arthrodesis (**Fig. 3**). The fused STT complex exhibits notable stress concentrations, particularly at its articulation with the radius. From the volar view, the unified STT bone complex actively participates in proximal-distal force transfer, with stress values between 5-7 MPa observed throughout the fused complex. The capitate's distal portion shows significant stress concentration, indicating its key role in load transmission, while the lunate, hamate, and triquetrum demonstrate comparatively lower stress values (2-4 MPa), with concentration primarily at ligament attachment sites.

From the dorsal perspective, stress distribution appears more uniform across the carpal bones, without pronounced stress concentrations observed in the healthy model. The fused STT bone complex displays a more continuous stress pattern throughout its structure compared to the individual behavior observed in the unfused bones. The upper limit shown in the legend was manually set to 10 MPa, corresponding to 99.20% of the elements in the model; this value was chosen to ease comparison with the healthy model.



a)



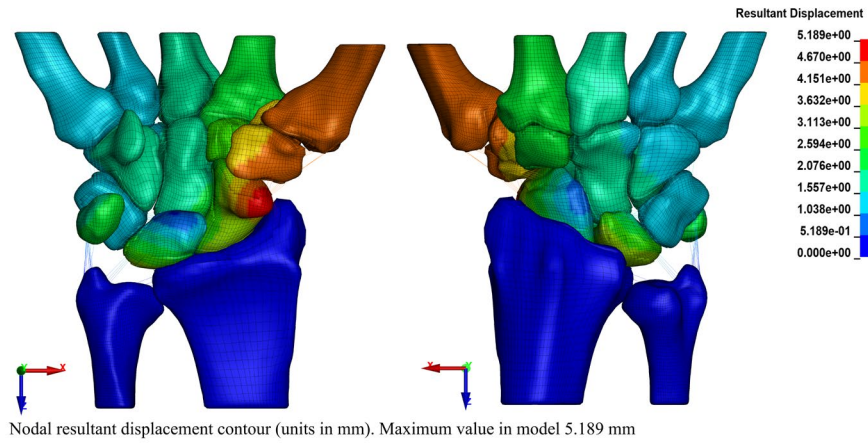
b)

Fig. 3. Stress contours for metacarpal-based grasping: a) healthy model and b) STT fusion model. Volar (left) and dorsal (right) views.

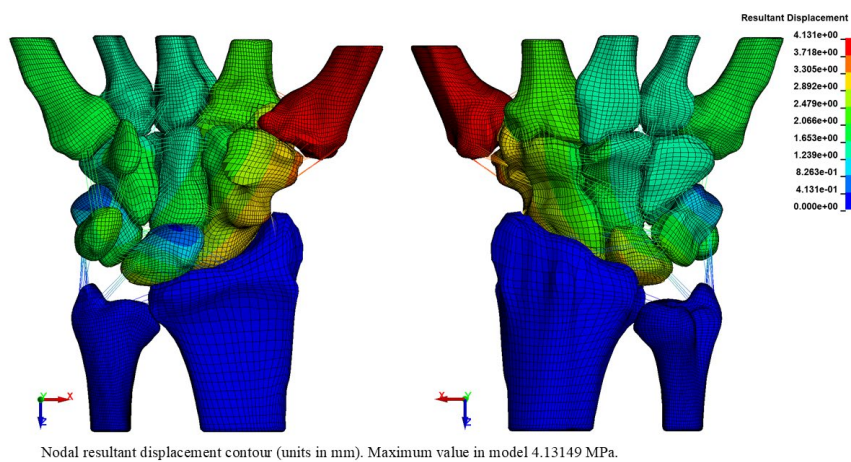
Displacement contours (**Fig. 4**) demonstrate altered behavior (vs. the healthy case) following STT fusion. The first metacarpal (MC1) exhibits the largest displacement (approximately 4 mm), indicating thumb mobility remains relatively unimpaired despite trapezium fusion. The fused STT complex shows regionally varied displacement patterns, suggesting some degree of rotation about its articulation with the capitate, where displacement values remain below 2 mm.

The central column of the wrist (MC3, MC4, and capitate) maintains its stability with minimal displacement, consistent with observations in the healthy model. The

distal carpal row continues to function as a cohesive unit, while the proximal row bones (excluding the now-fused scaphoid) retain their individual mobility characteristics. The preservation of this behavior suggests that STT fusion has local biomechanics effects, but it does not drastically alter the displacement patterns of the healthy wrist model.



a)



b)

Fig. 4. Displacement contours for metacarpal-based grasping: a) healthy model and b) STT fusion model. Volar (left) and dorsal (right) views.

4 Discussion

Our finite element analysis reveals significant biomechanical adaptations following STT arthrodesis. Comparing the STT fusion model with the previously validated healthy wrist model [14], several differences are noted in load distribution patterns, stress concentrations, and displacement characteristics.

The overall radial force transfer slightly increased following STT fusion (from 86.05% to 87.98%), indicating that the radial pattern of axial load transmission is preserved. However, this finding contrasts with the observed substantial reduction in peak contact pressures at the radioscaphoid (49.3% decrease) and radiolunate (12.0% decrease) articulations. This apparent discrepancy can be explained by examining the altered stress distribution throughout the carpus.

In the healthy wrist, the capitate serves as the primary load-bearing structure, with stress distributed throughout its entire body before transferring to the proximal row and ultimately to the radius [14]. Following STT fusion, the unified STT bone complex becomes a major participant in load transfer, exhibiting significant stress concentrations, particularly at its articulation with the radius. The capitate's role changes, with stress concentrations now visible in its distal portion rather than force transfer throughout the entire bone. This suggests a redistribution of the load path, where forces travel through the fused STT complex via multiple directions rather than primarily through the capitate as observed in the healthy wrist.

The von Mises stress contours show that while overall load distribution maintains its radial preference, the specific direction through which these forces travel is modified. The stress patterns in the fused STT complex appear more uniform than the individual behaviors observed in the unfused (healthy case) bones. This redistribution explains why radial force transmission can increase while radiocarpal contact pressures decrease: the load is distributed over a larger area of the radio-STT interface rather than concentrated at specific articulation points.

Displacement patterns also help us understand the biomechanical consequences of STT fusion. Maximum nodal displacement decreased from 5.19 mm in the healthy model to 4.13 mm in the STT fusion model, consistent with the expected reduction in mobility following arthrodesis [1], [23], [24]. The location of maximum displacement shifted from the scaphoid distal tubercle in the healthy model to the first metacarpal (MC1) in the fusion model. The fused STT complex behaves as a single column, moving with slight rotation but without the independent mobility seen in the separate bones of the healthy model. Despite this constraint, the central column of the wrist (MC3, MC4, and capitate) maintains its stability with minimal displacement in both models.

These findings align with the expected biomechanical consequences of arthrodesis procedures, which typically sacrifice some mobility to enhance stability [23], [24]. However, the observation that significant motion remains at the first metacarpal could suggest that thumb functionality might not be that compromised, though it should be noted that our simulation represents an idealized case and may not fully capture the reduced capabilities of a post-surgical wrist, besides the original limitations of the healthy model when it comes to soft tissues.

Our findings contribute to the limited computational works on wrist arthrodesis procedures. To date, few FE studies have investigated the biomechanical effects of carpal fusion techniques, and to our knowledge, this study presents the first computational analysis of STT arthrodesis.

When compared with other computational studies of wrist surgeries, our approach offers insights into bone fusion interventions. Faudot et al. (2021) examined four-corner fusion (FCF), a more extensive procedure involving scaphoid excision and fusion of the lunate, capitate, hamate, and triquetrum [23]. Their study showed that FCF aims to eliminate motion between the carpal rows, creating a single stable block of bones that moves as a unit relative to the radius. In contrast, STT fusion preserves much of the natural load transfer mechanisms while stabilizing only one carpal column (scaphoid, trapezium, trapezoid). The biomechanical advantage of STT fusion appears to be its ability to maintain radial load transmission while redistributing forces more evenly across the radiocarpal interface, potentially reducing localized stress concentrations at critical articulations. Moreover, a scaphoidectomy is not required in this case, so the radioscaphoid articulation is preserved.

Other computational studies focus on total wrist arthroplasty (TWA) [25], representing a more radical intervention with complete alteration of load transfer mechanics. Unlike TWA, the STT fusion model preserves natural bone structures and articulating surfaces at critical load-bearing interfaces, allowing for a more physiological stress distribution pattern.

Our results align with experimental findings from Short et al. [13], who demonstrated using a cadaver model that STT joint fusion with the scaphoid in a neutral position unloads the lunate fossa and shifts load to the radioscaphoid joint. Our computational model supports this observation, showing reduced contact pressure at the radiolunate articulation along with altered stress patterns in the capitate, where forces are more concentrated in its distal portion compared to the uniform distribution seen in the healthy model.

It is important to acknowledge the limitations of this study. As with most computational models of surgical interventions, our analysis does not capture all details of pathological conditions that might require a procedure like STT arthrodesis. The challenges of accurately modeling wrist arthritis—which is multifactorial and characterized by substantial changes in geometry, material properties, and soft tissues [26]—prevent us from simulating specific disease stages. Instead, our model represents an idealized scenario after successful fusion has been achieved, focusing on the long-term biomechanical consequences rather than the immediate post-surgical condition.

Additionally, our model is based on a type I wrist, and the results cannot be directly extrapolated to type II wrists, where the capitate-hamate-lunate interactions differ significantly and would likely alter load transfer patterns [15], [16]. Furthermore, we have focused exclusively on static loading during grasping, which represents only one aspect of wrist function. Future work could explore different wrist motions to better understand how STT fusion affects the functional range of motion.

Despite these limitations, our findings provide initial biomechanical evidence that confirms our hypothesis: STT joint arthrodesis significantly affects the transfer of forces through the radiocarpal joint, as evidenced by the substantial reductions in peak

contact pressures at both the radioscaphoid (49.3% decrease) and radiolunate (12.0% decrease) articulations. Additionally, our results demonstrate that the midcarpal joint structure does indeed influence force transfer patterns, with the fused STT complex becoming a primary load-bearing structure and altering the stress distribution in the capitate. From a clinical perspective, these biomechanical changes support STT arthrodesis as a viable option for certain wrist conditions. The preservation of radial force transmission with reduced radiocarpal contact pressures suggests that this procedure may offer long-term joint preservation while maintaining key aspects of normal wrist biomechanics. This aligns with the clinical objective of achieving a stable, pain-free wrist without excessively compromising function.

References

- [1] H. K. Watson, "Limited wrist arthrodesis.," *Clin Orthop Relat Res*, no. 149, pp. 126–36, Jun. 1980.
- [2] L. Obert *et al.*, "Scaphotrapeziotrapezoid osteoarthritis: From the joint to the patient," *Hand Surg Rehabil*, vol. 40, no. 3, pp. 211–223, Jun. 2021, doi: 10.1016/j.hansur.2020.12.007.
- [3] B. Acar, A. Turan, O. Kose, S. Ozturk, and M. Sindel, "Scaphotrapeziotrapezoid Arthrodesis Using Limited Wrist Fusion Plates in Kienböck's Disease," *Cureus*, Feb. 2019, doi: 10.7759/cureus.4025.
- [4] J. Myllykoski, M. P. Räisänen, T. Kotkansalo, M. Juntunen, and M. Pääkkönen, "Arthroscopic Scaphotrapeziotrapezoid Joint Fusion for Osteoarthritis," *J Hand Surg Asian Pac Vol*, vol. 28, no. 05, pp. 580–586, Oct. 2023, doi: 10.1142/S2424835523500613.
- [5] H. K. Watson and R. F. Hempton, "Limited wrist arthrodeses. I. The triscaphoid joint," *J Hand Surg Am*, vol. 5, no. 4, pp. 320–327, Jul. 1980, doi: 10.1016/S0363-5023(80)80169-9.
- [6] S. K. Rhee, H. M. Kim, W. J. Bahk, and Y. W. Kim, "A comparative study of the surgical procedures to treat advanced Kienbock's disease," *J Korean Med Sci*, vol. 11, no. 2, p. 171, 1996, doi: 10.3346/jkms.1996.11.2.171.
- [7] W. D. Rogers and H. Kirk Watson, "Degenerative arthritis at the triscaphe joint," *J Hand Surg Am*, vol. 15, no. 2, pp. 232–235, Mar. 1990, doi: 10.1016/0363-5023(90)90100-6.
- [8] W. B. Kleinman, "Long-term study of chronic scapho-lunate instability treated by scapho-trapezio-trapezoid arthrodesis," *J Hand Surg Am*, vol. 14, no. 3, pp. 429–445, May 1989, doi: 10.1016/S0363-5023(89)80002-4.
- [9] M. Cholley-Rouleau, F. Dap, G. Dautel, and L. Athlani, "Scaphotrapeziotrapezoid arthrodesis for isolated osteoarthritis: results at a mean 8 years' follow-up," *Hand Surg Rehabil*, vol. 40, no. 5, pp. 602–608, Oct. 2021, doi: 10.1016/j.hansur.2021.04.014.
- [10] M. J. Rogers *et al.*, "Scaphotrapeziotrapezoid Arthrodesis: A 10-Year Follow-up Study of Complications in 58 Wrists," *HAND*, vol. 17, no. 5, pp. 919–925, Sep. 2022, doi: 10.1177/1558944720964972.

- [11] M. Garcia-Elias and A. Lluch, "Partial excision of scaphoid: is it ever indicated?," *Hand Clin*, vol. 17, no. 4, pp. 687–95, x, Nov. 2001.
- [12] M. Cholley-Rouilleau, G. Dautel, F. Dap, G. Hossu, P. Bellemère, and L. Athlani, "Comparison between scaphotrapeziotrapezoid arthrodesis and Pyrocardan® implant for isolated scaphotrapeziotrapezoid osteoarthritis," *Orthopaedics & Traumatology: Surgery & Research*, p. 103867, Mar. 2024, doi: 10.1016/j.otsr.2024.103867.
- [13] W. H. Short, F. W. Werner, M. D. Fortino, and A. K. Palmer, "Distribution of pressures and forces on the wrist after simulated intercarpal fusion and Kienböck's disease," *J Hand Surg Am*, vol. 17, no. 3, pp. 443–449, May 1992, doi: 10.1016/0363-5023(92)90345-P.
- [14] A. Mena, R. Wollstein, and J. Yang, "Development of a Finite Element Model of the Human Wrist Joint With Radial and Ulnar Axial Force Distribution and Radiocarpal Contact Validation," *J Biomech Eng*, vol. 147, no. 3, pp. 1–39, Mar. 2025, doi: 10.1115/1.4067580.
- [15] K. Nakamura, R. M. Patterson, H. Moritomo, and S. F. Viegas, "Type I versus type II lunates: Ligament anatomy and presence of arthrosis," *J Hand Surg Am*, vol. 26, no. 3, pp. 428–436, May 2001, doi: 10.1053/jhsu.2001.24140.
- [16] S. F. Viegas, R. M. Patterson, J. A. Hokanson, and J. Davis, "Wrist anatomy: Incidence, distribution, and correlation of anatomic variations, tears, and arthrosis," *J Hand Surg Am*, vol. 18, no. 3, pp. 463–475, May 1993, doi: 10.1016/0363-5023(93)90094-J.
- [17] 3D Slicer, "3D Slicer image computing platform." Accessed: Feb. 13, 2024. [Online]. Available: <https://www.slicer.org/>
- [18] A. Fedorov *et al.*, "3D Slicer as an image computing platform for the Quantitative Imaging Network," *Magn Reson Imaging*, vol. 30, no. 9, pp. 1323–41, Nov. 2012, doi: 10.1016/j.mri.2012.05.001.
- [19] A. K. Palmer and F. W. Werner, "Biomechanics of the distal radioulnar joint.," *Clin Orthop Relat Res*, no. 187, pp. 26–35, 1984.
- [20] F. W. Werner, A. K. Palmer, M. D. Fortino, and W. H. Short, "Force transmission through the distal ulna: Effect of ulnar variance, lunate fossa angulation, and radial and palmar tilt of the distal radius," *J Hand Surg Am*, vol. 17, no. 3, pp. 423–428, May 1992, doi: 10.1016/0363-5023(92)90342-M.
- [21] M. K. Gislason *et al.*, "A three-dimensional finite element model of maximal grip loading in the human wrist," *Proc Inst Mech Eng H*, vol. 223, no. 7, pp. 849–861, Mar. 2009, doi: 10.1243/09544119jeim527.
- [22] M. H. Ramlee, G. K. Beng, N. Bajuri, and M. R. A. Kadir, "Finite element analysis of the wrist in stroke patients: the effects of hand grip," *Med Biol Eng Comput*, vol. 56, no. 7, pp. 1161–1171, Dec. 2017, doi: <https://doi.org/10.1007/s11517-017-1762-3>.
- [23] B. Faudot *et al.*, "Mechanical performance comparison of two surgical constructs for wrist four-corner arthrodesis via dorsal and radial approaches," *Clinical Biomechanics*, vol. 82, p. 105274, Feb. 2021, doi: 10.1016/j.clinbiomech.2021.105274.

- [24] H. A. Peterson, “Intercarpal Arthrodesis,” *Archives of Surgery*, vol. 95, no. 1, p. 127, Jul. 1967, doi: 10.1001/archsurg.1967.01330130129026.
- [25] M. K. Gislason, E. Foster, M. Bransby-Zachary, and D. H. Nash, “Biomechanical analysis of the Universal 2 implant in total wrist arthroplasty: a finite element study,” *Comput Methods Biomech Biomed Engin*, vol. 20, no. 10, pp. 1113–1121, Jun. 2017, doi: 10.1080/10255842.2017.1336548.
- [26] M. Garcia-Elias and A. Lluch, *Green’s Operative Hand Surgery*, 7th ed. Elsevier.